V European Conference on Computational Fluid Dynamics
ECCOMAS CFD 2010
J. C. F. Pereira and A. Sequeira (Eds)
Lisbon, Portugal,14-17 June 2010

SPECTRAL VOLUME METHOD: APPLICATION TO EULER EQUATIONS AND PERFORMANCE APPRAISAL

Oussama Chikhaoui, Jérémie Gressier and Gilles Grondin

Département d'Aérodynamique, Énergétique et Propulsion
Institut Supérieur de l'Aéronautique et de l'Espace
address 10 av. Edouard Belin - BP 54032 - 31055 Toulouse - FRANCE
e-mail: {oussama.chikhaoui, jeremie.gressier, gilles.grondin}@isae.fr

Key words: High-order methods, Spectral volume method, Unstructured grid, Compressible flows

Abstract. *The compact high-order 'Spectral Volume Method' (SVM, Wang (2002)) designed for conservation laws on unstructured grids is presented. Its spectral reconstruction is exposed briefly and its applications to the Euler equations are presented through several test cases to assess its accuracy and stability. Comparisons with usual methods such as MUSCL show the superiority of SVM. The SVM method arises as a high-order accurate scheme, geometrically flexible and computationally efficient.*

1 INTRODUCTION

Despite the constant improvements in computational and data processing ressources, the continuously growing requirements of computational fluid dynamics remain still unsatisfied. In the last decade, the CFD community showed a growing interest in high-order approximations for solving these issues (WENO, Discontinuous Galerkin, ...). An attractive choice is the *'Spectral Volume Method'* (SVM) proposed and developed by Wang et al.[1,2,3,4].

The SVM method achieves high-order accuracy on unstructured grids through polynomial reconstruction within initial grid cells (spectral volumes, SV) with a subdivision of the SV into polygonal control volumes (CV). The spectral splitting of the SV is designed to minimize internal reconstruction oscillations (Van den Abeele et al.[5,6]). Moreover, the reconstructed field is continuous over the entire SV, therefore internal faces are not Riemann problems. This property reduces the fluxes computation cost and contains the limiters problems to the SV interfaces. The flux computation is finally achieved with Gaussian quadrature directly inferred from CV states ponderation with a constant and unique set of coefficients for each SV in the whole domain.

To assess the performance of the SVM method, different test cases were computed with *Typhon*, an unstructured open-source code. The numerical experiments were chosen to cover a large set of flow configurations from continuous quasi-incompressible problems to shock wave propagations and mixing flows. Time integration is performed with a third order TVD Runge-Kutta scheme and SVM results are compared to results provided by classic schemes such as MUSCL.

The results are up to expectations with a significant increase in accuracy and a reduction in CPU time per cycle compared to a usual second order scheme method using the same number of control volumes.

2 Spectral Volume Method for the 2D Euler equations

We consider the two-dimensional Euler equations written in the conservative form on a domain Ω with appropriate initial and boundary conditions:

$$\frac{\partial Q}{\partial t} + \frac{\partial E}{\partial x} + \frac{\partial F}{\partial y} = 0 \tag{1}$$

with

$$Q = \begin{Bmatrix} \rho \\ \rho u \\ \rho v \\ e \end{Bmatrix}, \quad E = \begin{Bmatrix} \rho u \\ \rho u^2 + p \\ \rho uv \\ u(e+p) \end{Bmatrix}, \quad F = \begin{Bmatrix} \rho v \\ \rho uv \\ \rho v^2 + p \\ v(e+p) \end{Bmatrix}$$

The domain Ω is discretized into N nonoverlapping triangular cells S_i (Fig.1), called

spectral volumes (SV's), i.e.,

$$\Omega = \bigcup_{i=1}^{N} S_i$$

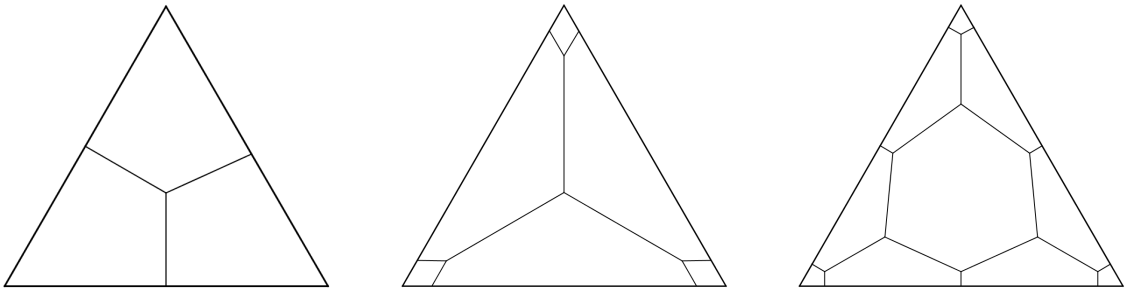

Figure 1: Examples of SV splitting into CVs for second, third and fourth order

If we fix a given approximation order k, every spectral volume S_i is then partitioned into $m = k(k+1)/2$ subcells, called control volume (CV's), i.e.

$$S_i = \bigcup_{j=1}^{m} C_{ij}$$

If q denotes a conservative variable of Q, the average value of q over a control volume is then defined as:

$$\overline{q}_{ij}(t) = \frac{\int_{C_{ij}} q(x,y,t)dxdy}{V_{ij}}, \qquad j = 1..m, \qquad i = 1..N \tag{2}$$

Let us consider known all the average values over a control volume C_{ij} in a given spectral volume S_i, we can build a polynomial $p_i(x,y)$ which is a k^{th} order polynomial approximation to the state variable, i.e.:

$$p_i(x,y) = q(x,y) + O(h^k), (x,y) \in S_i, \qquad i = 1..N \tag{3}$$

This reconstruction can be defined by the analytical resolution of:

$$\frac{\int_{C_{ij}} p_i(x,y)dxdy}{V_{ij}} = \overline{q}_{ij}(t), \qquad j = 1..m \tag{4}$$

The polynomial approximation can be expressed as:

$$p_i(x,y) = \sum_{j=1}^{m} L_j(x,y)\overline{q}_{ij}$$

where L_j are the shape functions, i.e. :

$$\frac{\int_{C_{ij}} L_l(x,y)dxdy}{V_{ij}} = \delta_{jl} \tag{5}$$

Such functions can be established analytically for a given partition of S_i. The shape functions for the fourth order SV scheme with Wang's partition is represented on figure 2.

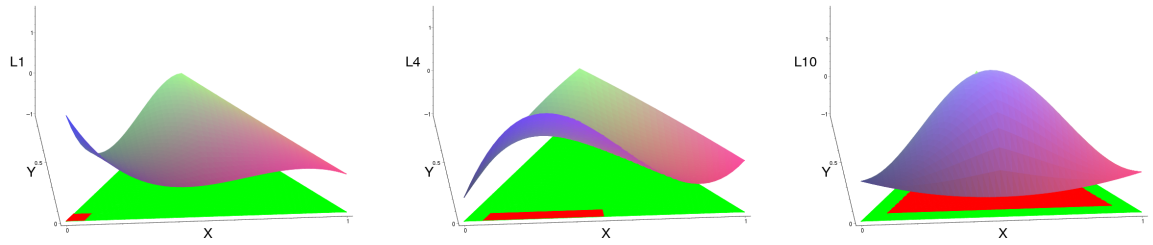

Figure 2: Shape functions for fourth order SV with Wang's partition

The high order reconstruction is then used to update average variables on CV. Integration of equation 1 on a control volume CV gives:

$$\frac{d\overline{Q}_{ij}}{dt} + \frac{1}{V_{ij}} \sum_{r=1}^{K} \int_{A_r} (f \cdot \mathbf{n}) dA = 0 \tag{6}$$

where K is the number of faces in C_{ij} and A_r the r^{th} face. The integration on each face can be performed whith a k^{th} order accurate Gauss quadratic formula, i.e. :

$$\int_{A_r} (f \cdot \mathbf{n}) dA = \sum_{q=1}^{J} w_{rq} f(Q(x_{rq}, y_{rq})) \cdot \mathbf{n_r} A_r + O(A_r h^k) \tag{7}$$

$J = int((k+1)/2)$ is the number of quadrature points per face, w_{rq} are the Gauss quadrature weights and (x_{rq}, y_{rq}) are the coordinates of Gauss points. Therefore, the following semi-discrete equation is obtained:

$$\frac{d\overline{Q}_{ij}}{dt} + \frac{1}{V_{ij}} \sum_{r=1}^{K} \sum_{q=1}^{J} w_{rq} f(Q(x_{rq}, y_{rq})) \cdot \mathbf{n_r} A_r = 0 \tag{8}$$

Finally, the resolution is achieved using a usual time integration method.

2.1 Spectral volumes partitions

The subdivision of a spectral volume S_i in different controle volumes C_{ij} is an essential step for the SVM scheme. For example, some geometric partitions can lead to degenerated systems and thus should be excluded. The splitting procedure must conserve the existing symmetries in a triangle, use straight edges and consider convex control volumes CVs. Fig. 3 shows different geometric partitions of a spectral volume SV for different desired orders. While the second order splitting definition is unique, the higher order partitions introduce some geometric parameters. The third order partitions is defined by two parameters: $\alpha = \frac{AD}{AB}$ and $\beta = \frac{AF}{AA1}$. The fourth order partitions have four degrees of freedom: $\alpha = \frac{AD}{AB}$, $\beta = \frac{AG}{AR}$, $\gamma = \frac{OR}{AR}$ and $\delta = \frac{AL}{AR}$. The accuracy and stability of a given spectral volume scheme depends on the choice of these geometric parameters (Abeele at al.[5]).

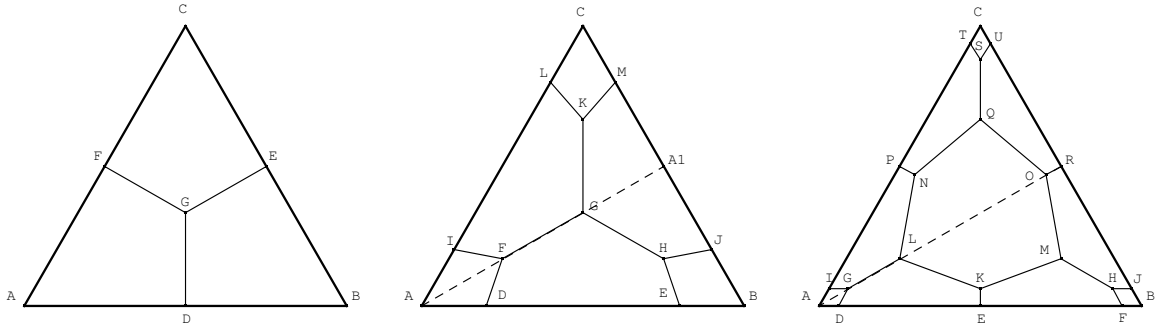

Figure 3: Geometric splitting definitions for the second, third and fourth order partitions

Table 1 sums up the different implemented and tested partitions with their geometric parameters.

Partition	Order	α	β	δ	γ
SVM2	2	-	-	-	-
SVM3W	3	1/4	1/3	-	-
SVM3K	3	91/1000	18/100	-	-
SVM3K2	3	0.1093621117	0.1730022492	-	-
SVM4W	4	1/15	2/15	2/15	1/15
SVM4K	4	78/1000	104/1000	52/1000	351/1000
SVM4K2	4	0.0326228301	0.042508082	0.0504398911	0.1562524902

Table 1: Geometric parameters for the different SVM partitions

The SVMW splittings were proposed by Wang et al. and they were designed by minimizing the Lebesgue constant over the SV. Whereas the minimization of this constant provides a good assessment of the quality of the SVM splitting, different observations

show that it is not a sufficient condition for the stability of the scheme. Thus, Abeele[5,6] proposed other geometric splittings noted as SVMK and SVMK2.

2.2 Spectral volume method assets

The spectral volume method uses a compact stencil which is a great advantage compared to other high order reconstructions. The latter methods are often based on projections and gradients evaluations on a quite large region of neighboring cells, which is rapidly prohibitive in terms of computational ressources (memory, CPU time) and can lead to accuracy deterioration, for example with stretched unstructured cells or near boundaries.

The SVM geometric splitting is designed and optimised in a spectral way to minimize internal reconstruction oscillations known as Runge phenomena (Fig.4). The reconstructed field is continuous over the entire SV, therefore internal faces are not Riemann problems, which reduces the flux computation cost and contains the problem of data limitation to the SVs faces. The other interesting aspect of the SVM is the fact that the

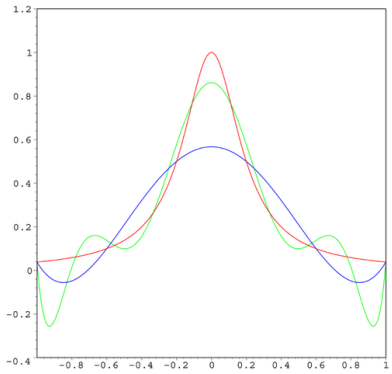

Figure 4: Runge phenomenon

splitting reconstruction is homothetic: no new metric terms need be kept in memory. The interpolation on Gauss points for fluxes computation is directly inferred from a weighting of CV states with constant and unique coefficients for the whole domain.

Lastly, while the usual finite-volume and finite-difference methods depend strongly on the grid quality and density, the SVM reconstruction remains exact (at a given order) on arbitrarily shaped triangles.

3 Numerical experiments

To assess the performance of the SVM method, different test cases were computed with *Typhon*[7], an unstructured open-source code. The numerical experiments were chosen to cover a large set of flows configurations, from continuous quasi-incompressible problems, to shock wave propagations and mixing flows. Time integration is performed with a third order TVD Runge-Kutta scheme and SVM results are compared to results provided by usual schemes such as MUSCL.

3.1 Vortex evolution problem

The first test case is a simple steady vortex evolution governed by the equation:

$$\frac{\partial p}{\partial t} = \rho \frac{{v_\theta}^2}{r} \tag{9}$$

with initial conditions set to :

$$p = 10^5 - 1.161 \cdot \frac{30^2}{2} \cdot \exp\left(1 - \frac{r^2}{4}\right)$$

An overview of the grids obtained after the SVM splitting procedure are presented on figure 5. The meshes were designed to have the same total number of CVs. The third-order TVD Runge-Kutta scheme was used for time integration.

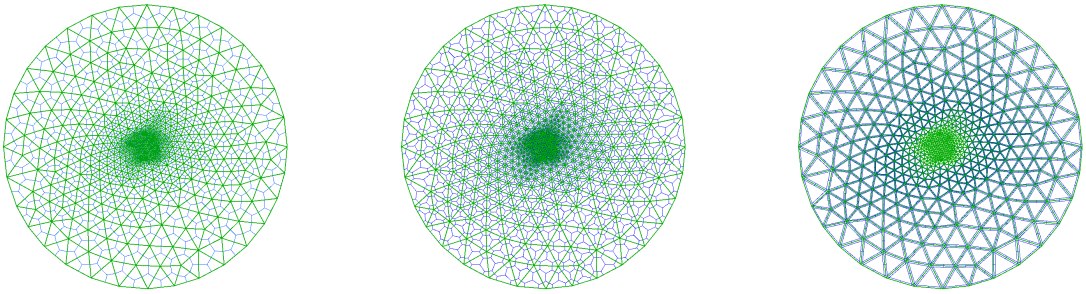

Figure 5: Controle volumes for the second, third and fourth order SV schemes

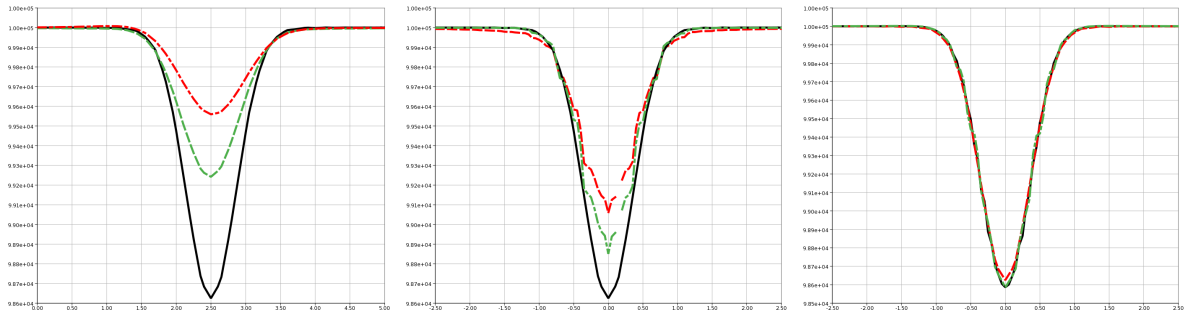

Figure 6: Pressure profiles at different times (t=0 in black, t=2 in green, t=10 in red): SVM2 (left), SVM3K (middle) et SVM4W (right)

Figure 6 shows pressure profiles across a line passing through the vortex center at $t = 0$, $t = 2$ and $t = 10$ for different SVM orders. The second order simulation produces a significant damping while the intensity in the vortex center is better conserved with the third order. With the fourth order, the peak of pressure is well resolved and preserved even with very long time simulations.

In order to assess the performance of the high-order SVM, the same test case has been performed on three different grids with the same number of SVs, using the usual MUSCL method and the fourth SVM scheme. Contours of pressure are shown on the figure 7. We can notice that even with the coarsest grid, composed of $(10 \times 10 \times 2)$ SV (i.e. 2000 CV for SVM4), the solution provided by the SVM scheme is more accurate than the MUSCL solution on the finest mesh (12800 CV).

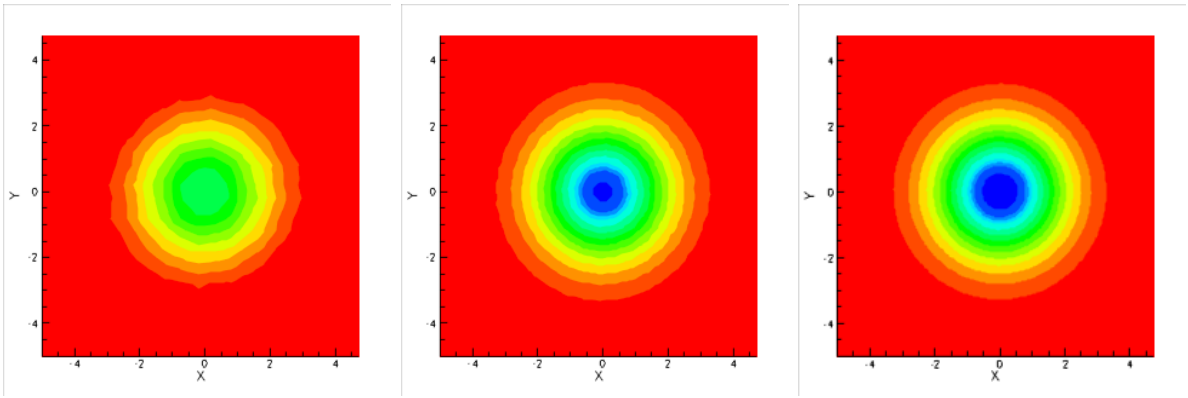

(a)

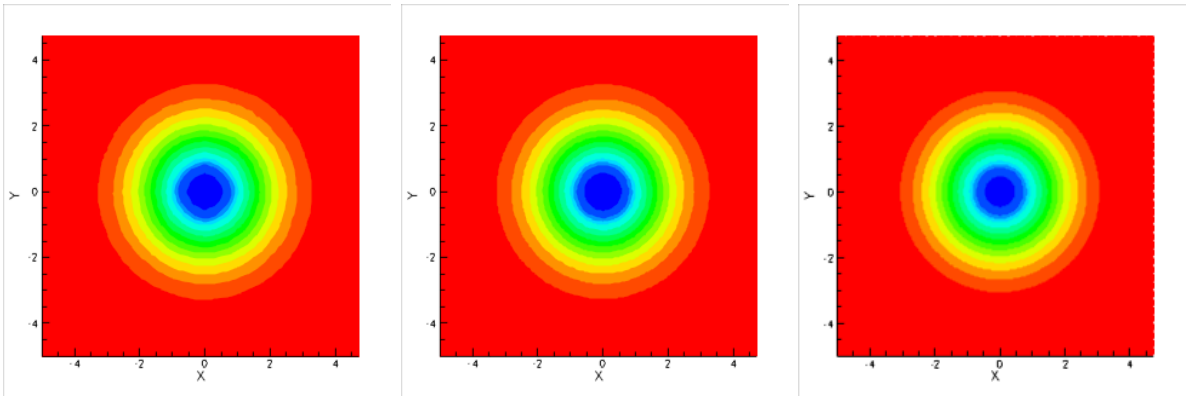

(b)

Figure 7: Pressure contours at t = 1s for different grids: $10 \times 10 \times 2$ (left), $40 \times 40 \times 2$ (middle) and $80 \times 80 \times 2$ (right). (a) : MUSCL (b) : SVM4.

Another interesting aspect of SVM simulations is the reduction in CPU time per cycle compared to a classic MUSCL method using the same number of control volumes (50% for 2^{nd} order, $32\% to 35\%$ for 3^{rd} order and $22\% to 25\%$ for 4^{th} order). The CPU savings are due to the absence of gradient evaluation for inviscid fluxes and the continuity of state variables through internal faces. This latter fact reduces the limitation problems and several cases can be computed without any limitation procedure.

3.2 Convected Vortex

In this test case, we consider the same vortex definition as in Eq. 9. However, the vortex is not steady in the domain center but convected with a speed of $V_{conv} = 20$ on a domain of $[10 \times 10]$. The boundary conditions are set to periodic in the x and y directions. No limiters were employed for the SVM simulations. For the following comparisons, the velocity profiles are considered along a horizontal line passing through the vortex center at $t = 1$: the vortex crosses the whole domain twice from left to right.

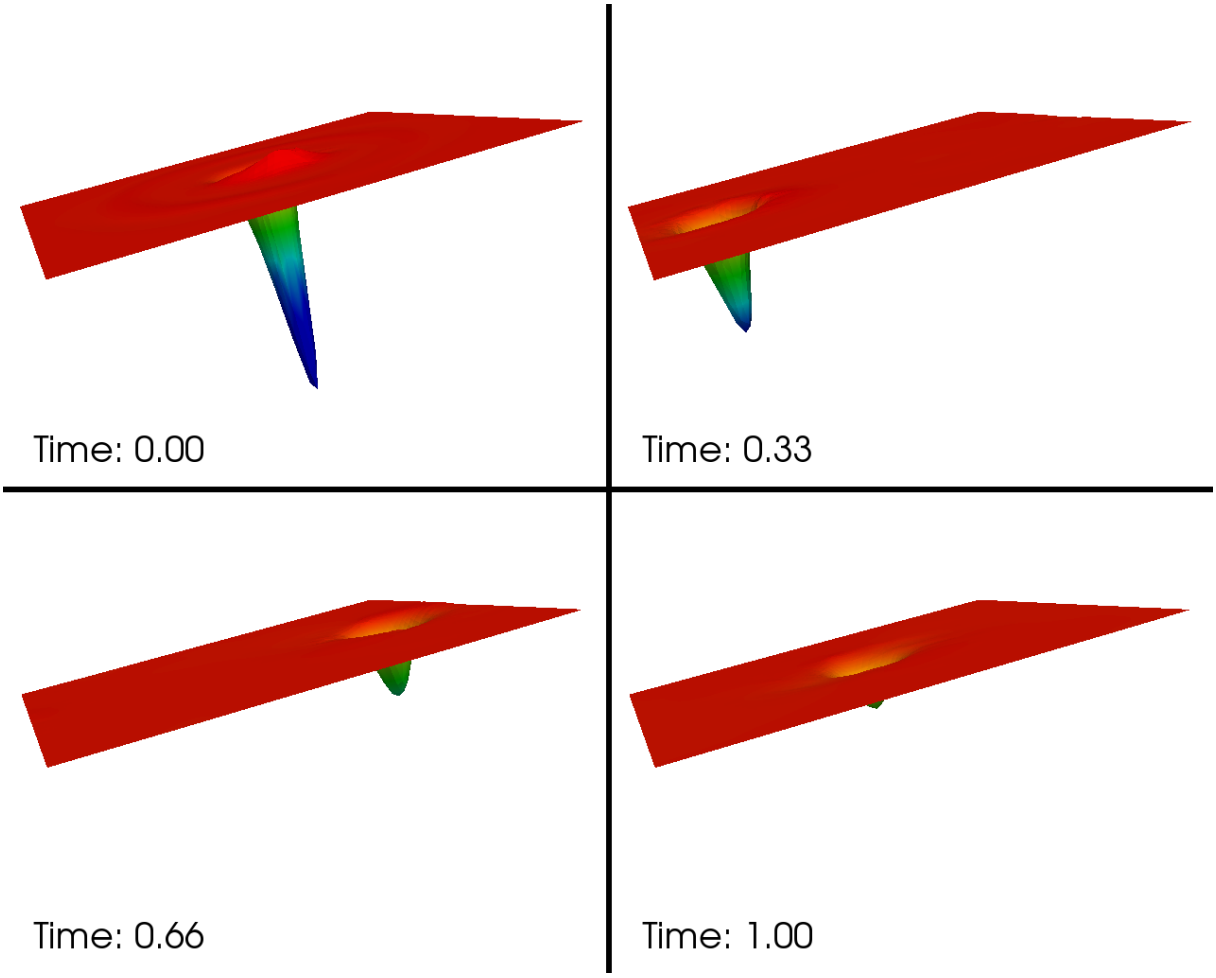

Figure 8: Overview of numerical damping of a convected vortex using MUSCL-Minmod scheme

Simulation with the classic MUSCL method are presented on figures 8 and 9 using the minmod and the Van Albada limiters. The results show the solution sensitivity to the limitation procedure. While the theoretical maximum transverse velocity is $V_{ymax} = 30$, $V_{ymax} \sim 10$ and $V_{ymax} \sim 15$ are respectively obtained for the minmod and the Van Albada simulations, which proves that this test case is very sensitive to numerical dissipation.

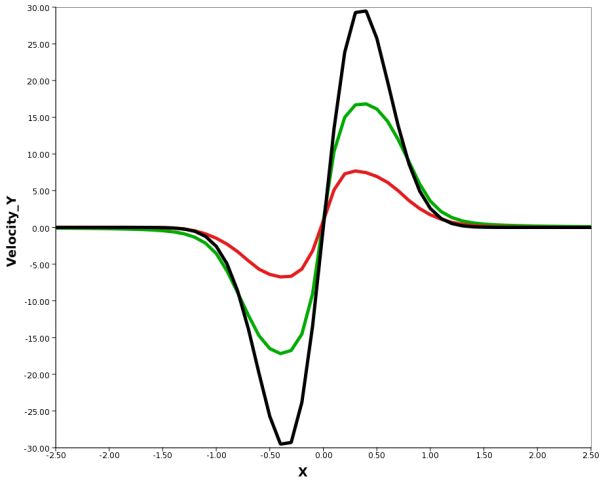

Figure 9: Comparison of velocity profiles from MUSCL simulations with the theoretical solution (black): Minmod limiter (red) and Van Albada limiter (green).

With the SVM schemes, the velocity profile is better preserved when the order is increased (Fig.10) . Thus, $V_{ymax} \sim 15$, $V_{ymax} \sim 25$ and $V_{ymax} \sim 30$ are obtained for the second, third and fourth order respectively.

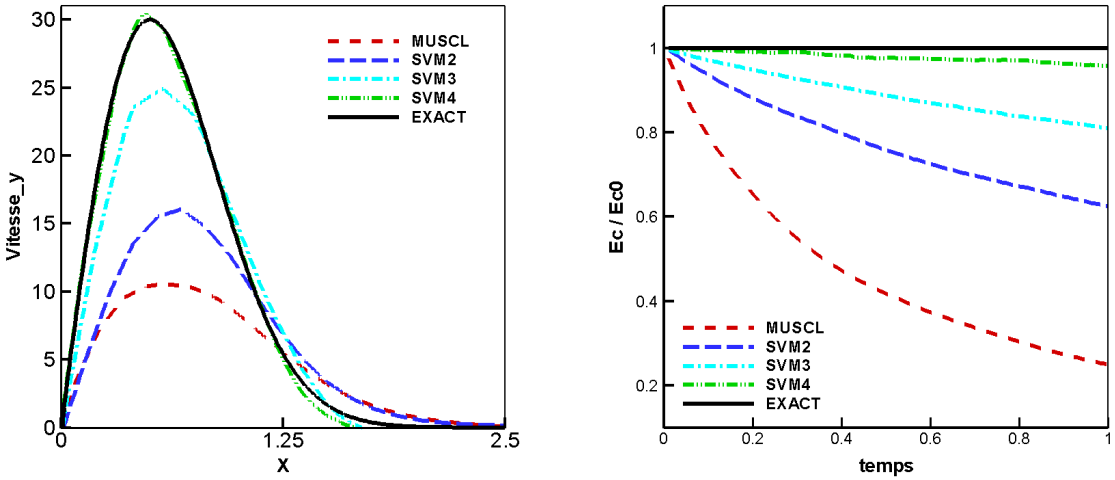

Figure 10: Comparison of velocity profiles along a line through the vortex center at $t = 1$ (left) and kinetic energy time evolution (right)

3.3 Simple Mach reflection

This case deals with a classic problem of shock reflection with a Mach number $M_s = 1.7$ and a wedge angle of $\theta = 25°$. The numerical results were obtained on a domain of $[25 \times 16.5]$ on the $x - y$ plane with the apex of the wedge placed at $x = 4.69$. The upstream shock conditions are ambient conditions, with $\rho_a = 1.225$, $p_a = 1.01325 \cdot 10^5$ and $u = 0$. The Riemann solver used is HLLC. All simulations were carried with the TVD RK-3 time integration scheme and a $CFL = 0.5$.

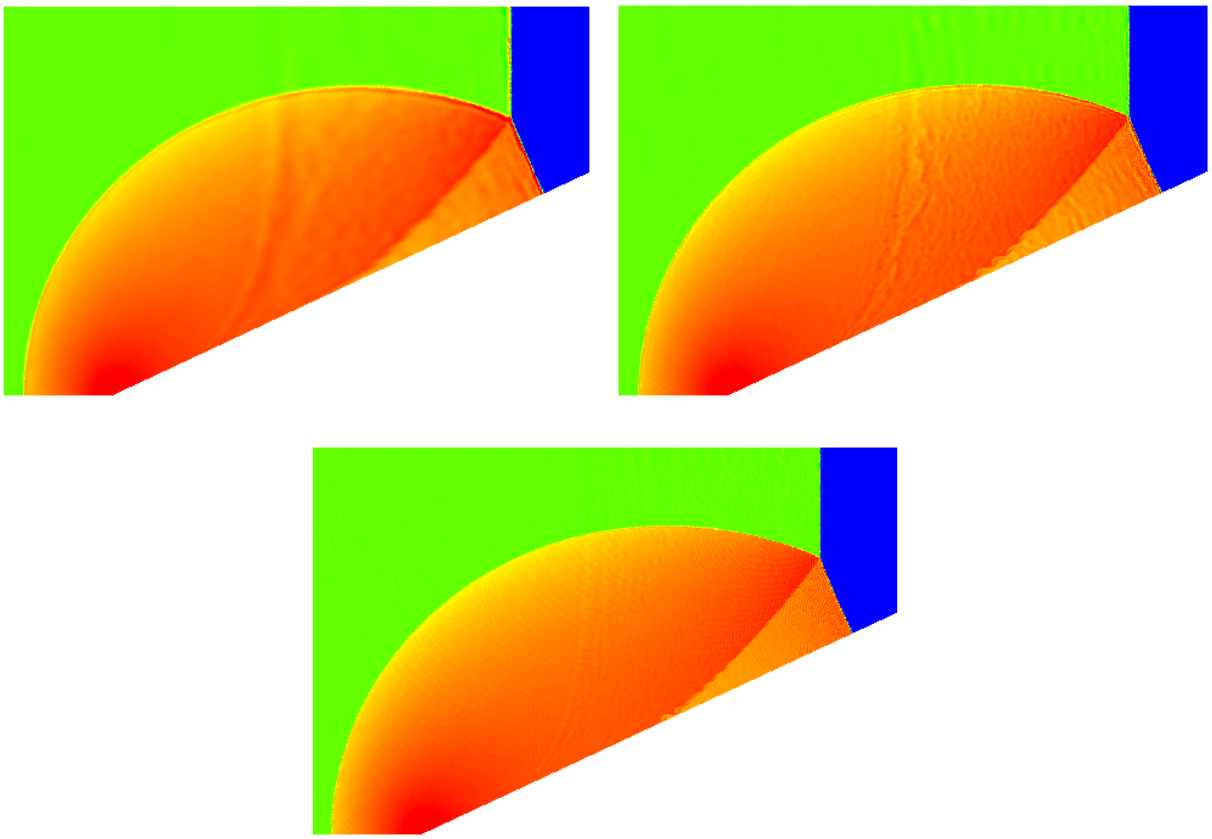

Figure 11: Density contours for SVM2, SVM3 and SVM4 simulations

Different experimental and computational results describe the solution to this problem. They show three shocks meeting at the triple point, namely, the incident shock, the reflected shock and the Mach stem. From the triple point emerges a slip surface that joins the wedge at a sharp angle. Different authors point out that the delicate feature for numerical simulations is the capture of this slip surface across which discontinuities in density and velocity occur (Toro[8]).

Density contours provided by different SVM simulations are shown on figure 11 . The

initial grid is an unstructured mesh with 42208 SVs: i.e. 126624 CVs for SVM2, 253248 CVs for SVM3 and 422080 CVs for SVM4. All SVM simulations for this case were carried with no limitation procedure.

It can be notices that the thicknesses of incident and reflected shocks are larger in the SVM2 solution, while it is well resolved for the SVM3 and SVM4. The contours around the slip surface are better captured when the order increases and the SVM4 solution clearly displays the development of instabilities near the wedge.

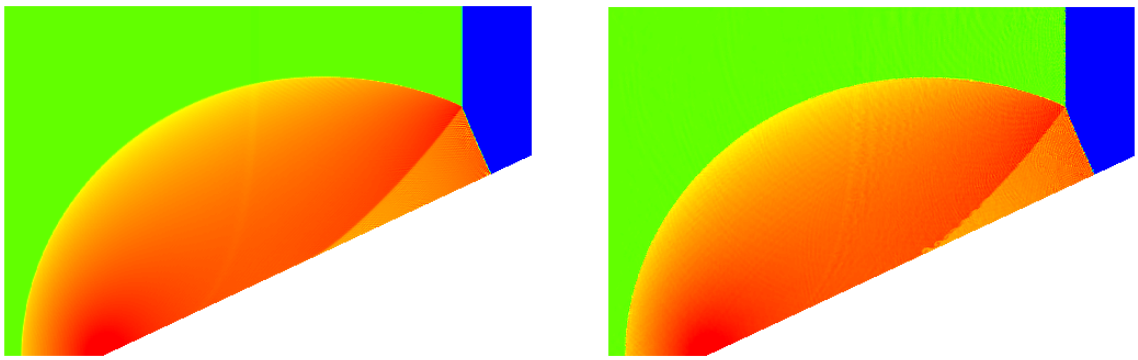

Figure 12: Density contours: MUSCL, 800.000 CV (left) and SVM4, 422.080 CV (right)

To prove that the capture of these features and the better resolution of the flow are due to the increasing order, other simulations have been undertaken using the MUSCL scheme.

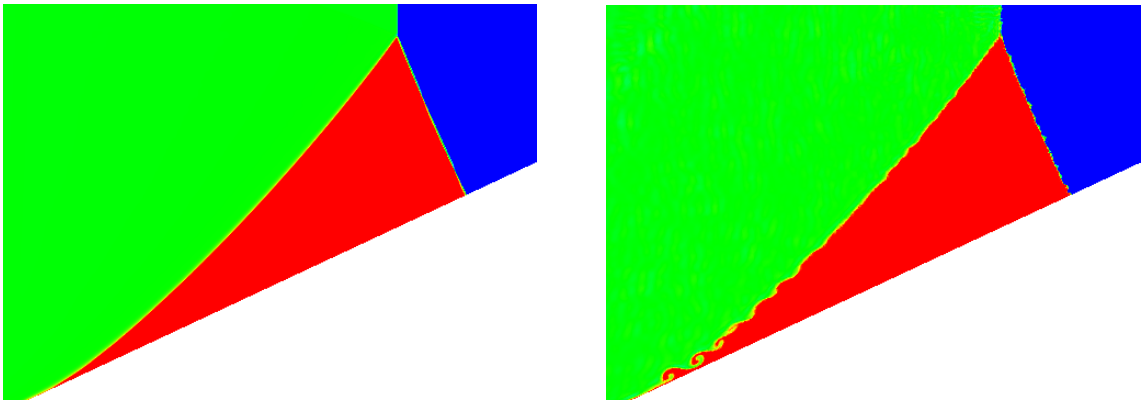

Figure 13: Entropy contours at slip surface: MUSCL, 800.000 CV (left) and SVM4, 422.080 CV (right)

The results obtained with the SVM4 scheme were compared to those provided by the MUSCL method on a structured cartesian finer grid (Fig.12). While the unstructured grid for SVM4 contains 422.080 CVs, the grid used for MUSCL simulation is a structured mesh

with twice the number of CVs, i.e. 800.000 CVs. Yet, the shocks thicknesses obtained are large and no improvement of the slip surface resolution is observed when increasing the number of CV with MUSCL method. Figure 13 clearly shows that the SVM scheme better captured the slip surface: Kelvin-Helmholtz instabilities can be noticed on the shear line. These observations suggest that the better resolution of the problem is achieved by the order increase rather than the mesh refinement.

3.4 Double Periodic Shear Layer

Finally, the problem of a double periodic shear layer is considered over a domain $[0,1] \times [0,1]$. The velocity is defined as shown on figure (Fig.14) with a smooth transition between layers and a 5% vertical pertubation.

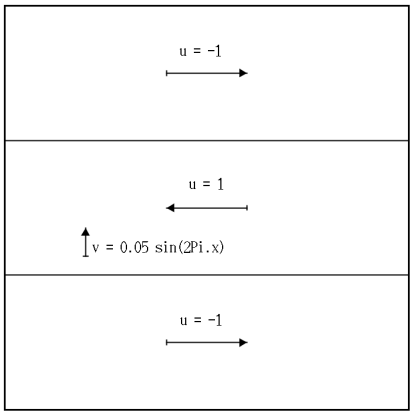

Figure 14: Case configuration and velocity initialisation

Initial density profile is defined by :

$$\rho = 1 + \frac{3}{2}\left(1 + tanh(30 \cdot (\frac{1}{4} - |Y - \frac{1}{2}|)\right)$$

Boundary conditions are set to be periodic in both x and y directions.

Figure 15 shows the time evolution of density contours for the third-order SVM scheme simulation over four adjacent domains. Though the field undergoes a single excitation, instabilities of different wavelengths form over time.

This test case is very sensitive to numerical schemes diffusion (Drikakis[9]), and some simple creterion could be used as a measure of the error in the computation such as the decay of kinetic energy. Figure 16 shows that the SVM schemes better conserve the total kinetic energy while the MUSCL simulations appear very dissipative.

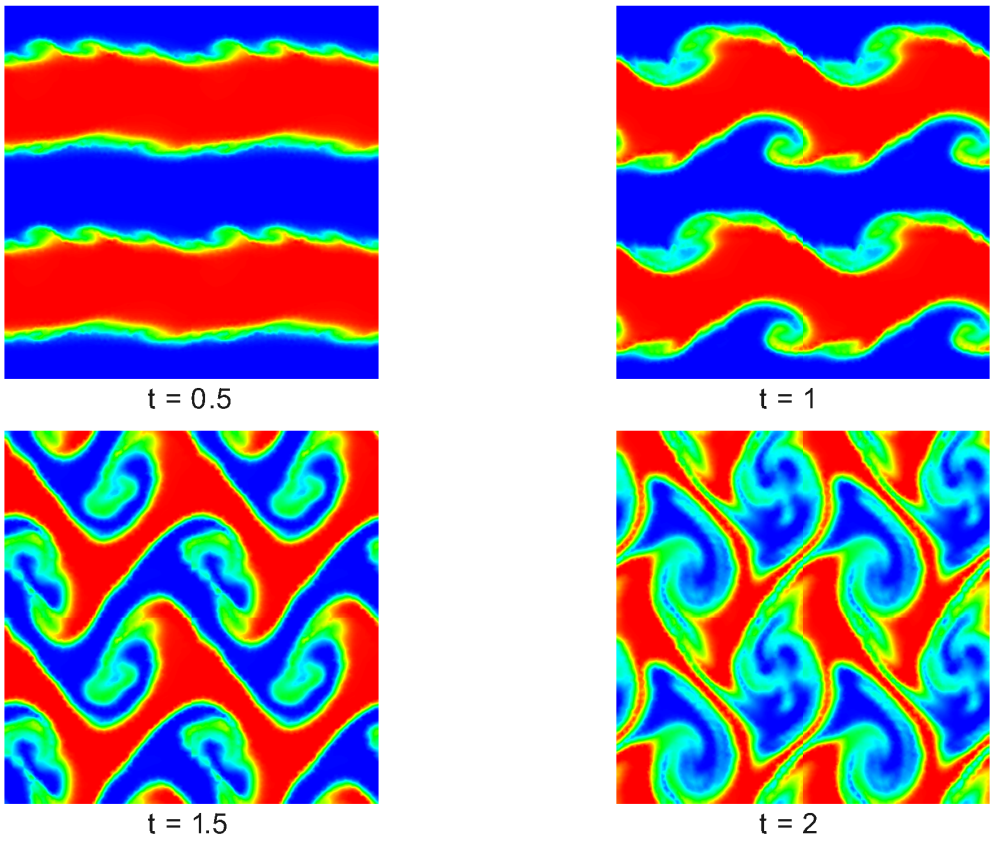

Figure 15: Density Contours

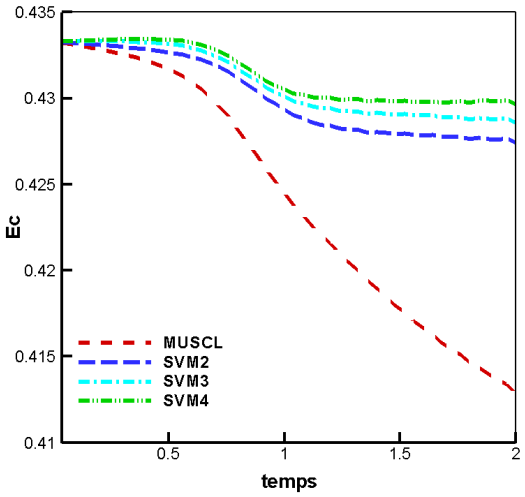

Figure 16: Double periodic shear layer: comparison of time evolution of the kinetic energy

4 Conclusion

In this study, analysis and applications of the Spectral Volume Method were presented. This high-order reconstruction is particularly interesting due to its compact support. Using splitted control volumes with flux evaluation remains quite close to the classic Finite-Volume method which keeps the SVM implementation in existing codes relatively easy.

The results are up to expectations with a significant increase in occuracy and a reduction in CPU time compared to a MUSCL method with the same number of elements (50% for 2^{nd} order, $32\%to35\%$ for 3^{rd} order and $22\%to25\%$ for 4^{th} order). The CPU gains are due to the absence of gradient evaluation for inviscid fluxes and the continuity of status variables through internal faces. This property reduces the limitation problems and several cases can be computed with no limitation procedure.

For all previously reported assets, the Spectral Volume Method arises as a promising high-order reconstruction device for both academic and industrial studies especially for complex applications which require great accuracy with computational ressources savings.

Investigations in the exentension of this method to viscous flows are currently under study. Different original choices and their implementation will be discussed in the future.

REFERENCES

[1] Z. J. Wang. Spectral (finite) volume method for conservation laws on unstructured grids. basic formulation: Basic formulation. *Journal of Computational Physics*, 178(1):210–251, May 2002.

[2] Z. J. Wang and Y. Liu. Spectral (finite) volume method for conservation laws on unstructured grids: Ii. extension to two-dimensional scalar equation. *Journal of Computational Physics*, 179(2):665–697, July 2002.

[3] Z. J. Wang, L. Zhang, and Y. Liu. Spectral (finite) volume method for conservation laws on unstructured grids iv: extension to two-dimensional systems. *Journal of Computational Physics*, 194(2):716–741, March 2004.

[4] Y. Sun, Z.J. Wang, and Y. Liu. Spectral (finite) volume method for conservation laws on unstructured grids vi: Extension to viscous flow. *Journal of Computational Physics*, 215(1):41–58, June 2006.

[5] K. Abeele and C. Lacor. An accuracy and stability study of the 2d spectral volume method. *Journal of Computational Physics*, 226(2):1007–10026, May 2007.

[6] K., Abeele, M., Ghorbaniasl, M., Parsani, C., Lacor A stability analysis for the spectral volume method on tetrahedral grids *Journal of Computational Physics*, 228, pp. 257-265, 2009.

[7] Typhon, http://typhon.sourceforge.net/

[8] E. F. Toro. Riemann Solvers and Numerical Methods for Fluid Dynamics. Springer, 1999.

[9] D. Drikakis and W. Rider. *High-Resolution Methods for Incompressible and Low-Speed Flows*. Springer-Verlag, 2005.